THE JOURNAL OF PHYSICAL CHEMISTRY C

Article

pubs.acs.org/JPCC

# Size Evolution of the 2e-Superatom in Ligand-Protected Au Nanoclusters: $Au_2$-$(AuL)_{1-12}$ (L = Cl, SH, $SCH_3$, $PH_2$, and $P(CH_3)_2$)

Wangdan Liu and Longjiu Cheng*

Department of Chemistry, Anhui University, Hefei, Anhui 230601, People's Republic of China

Supporting Information

**ABSTRACT:** Ligand-protected gold (Au-L) nanoclusters have attracted much attention due to their unique properties, and the superatom concept as a significantly well-known concept to explain the electronic stability was suggested. Although there has been a lot of major progress in this field, size evolution of the superatom is still little known because of limited experimental data. To give a direct and overall view of size evolution of the superatom in Au-L clusters, the $Au_2$-$(AuL)_{1-12}$ (L = Cl, SH, $SCH_3$, $PH_2$, $P(CH_3)_2$) system is taken as a test case. The global minimum geometries are studied by using a method combining the genetic algorithm with density functional theory. The gold cores in these structures consist of $Au_3$, $Au_4$, $Au_5$, and $Au_6$ 2e-superatoms protected by staple motifs. The 2e-superatoms were confirmed by chemical bonding analysis using the adaptive natural density partitioning method. The aromatic properties of the center of these compounds have been explored by the nucleus-independent chemical shift method, which indicates that the superatoms are highly aromatic. This work gives a clear size evolution of the 2e-superatomic Au-L clusters with 1 to 12 ligands, which discovers the growth mechanism of Au-L clusters with different ligands.

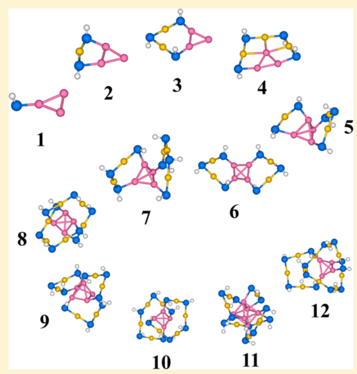


## 1. INTRODUCTION

Ligand-protected gold clusters have attracted interest both experimentally and theoretically over the past few years because of their unique electronic, optical, chemical, and catalytic properties.[1−10]

Numerous experimental studies have been devoted to the synthesis or characterization of ligand-protected gold nanoparticles in the size range of 1−2 nm.[11−15] The first major breakthrough in this field was achieved in 2007 for the crystallization and X-ray structure determination of the ($Au_{102}$(p-MBA)$_{44}$) gold nanoparticle.[13] They found that adatom-bound RS-Au-SR-type "staple" bonding motifs cover the surface of a $Au_{79}$ core in the stable $Au_{102}(SR)_{44}$ cluster, in agreement with the previous "divide-and-protect" model.[16] After one year, the second breakthrough was achieved in which the crystal structure of the $Au_{25}(SR)_{18}$ cluster was determined.[14,15] Then, $Au_{38}(SR)_{24}$,[17] $Au_{44}(SR)_{28}^{2-}$,[18] $Au_{36}(SR)_{23}$,[19] $Au_{19}(SR)_{13}$,[20] $Au_{18}(SR)_{14}$,[21] $Au_{68}(SR)_{32}$,[22] $Au_{30}S(SR)_{18}$,[23] $Au_{28}(SR)_{20}$,[24] $Au_{133}(SR)_{52}$,[25,26] and $Au_{44}(SR)_{28}$[27] compounds were experimentally isolated and characterized by the mass and/or optical spectra.

There are many theoretical ones devoted in this field. A great achievement was the prediction of the existence of the $Au_{25}(SR)_{18}$ nanoparticle.[28] On the basis of density functional theory (DFT), the structure of $Au_{25}(SR)_{18}$ was found to be a compact $Au_{13}$ core protected by six $(RS)_3Au_2$ complexes. The calculated X-ray diffraction (XRD) based on the predicted structure was in agreement with the experimental data. DFT is used in an implementation where the Kohn−Sham orbitals are expanded in Gaussian basis functions.[29] DFT predictions of the structures for many synthesized compounds were in agreement with the experimental X-ray diffraction and/or UV/vis spectra, successfully.[30−36] The structures of these clusters were all based on the "divide-and-protect" model.[16]

To understand the stability and electronic structures of these compounds, a significant known aspect which the superatom model of electronic stability obtained from the jellium theory was proposed.[37] For Au($5d^{10}6s^1$) clusters, the fully filled 5d electrons are mainly localized, and $6s^1$ are free valence electrons. The model states that the number of available Au 6s electrons must be a "magic number" such as 2, 8, 18, 34, 58, and 92. In particular, the total number of free valence electrons ($n^*$) associated with Au-SR clusters can be counted based on the formula $n^* = N_{vA} - M - z$, where $N_{vA}$ is the number of Au($6s^1$) electrons, $M$ the number of electron-localizing (or electron with drawing) ligands, and $z$ the overall charge on the complex. On the basis of this superatom model, the $n^*$ of the $Au_{102}(SR)_{44}$ compound was 58e, considered as a $Au_{79}$ core covered with 19 RS-AuSR and 2 RS-$(AuSR)_2$ staple motifs.[13] The superatom theory has achieved great success in the stability of many experimentally produced ligand-protected gold nanoparticles, which can be understood by the magic numbers, such as $Au_{68}(SR)_{34}$ (34e),[38] $Au_{44}(SR)_{28}^{2-}$ (18e),[18] $Au_{25}(SR)_{18}^-$ (8e),[15] and $Au_{12}(SR)_9^+$ (2e).[31]

In terms of Au-L nanoclusters, $Au_{15}(SR)_{13}$[7] and $Au_{11}(SR)_9$[39] compounds as 2e clusters have been experimentally isolated to

Received: October 29, 2015
Revised: January 14, 2016
Published: January 15, 2016

date. Jiang[40] predicted a novel structure model for $Au_{15}(SR)_{13}$ which features a cyclic [Au-SR] pentamer in the ligand shell, together with two regular trimer motifs protecting a $Au_4$ nucleus. Previously, three hypothetical formulas, $Au_{12}(SR)_9^+$,[31] $Au_{10}(SR)_8$,[41] and $Au_8(SR)_6$,[42] have been proposed to be candidates for the magic number 2. $Au_{12}(SR)_9^+$ has an octahedral ($Au_6$) core with three dimer motifs; $Au_{10}(SR)_8$ has a tetrahedral ($Au_4$) core with two interlocking trimer motifs; and $Au_8(SR)_6$ has a tetrahedral ($Au_4$) core protected by staple motifs. There are only a few reports about Au-L nanoclusters with the 2e-superatom. Some Au-L nanoparticles such as $Au_{18}(SR)_{14}$, $Au_{20}(SR)_{16}$, and $Au_{24}(SR)_{20}$ can be explained as a 2e-superatom based on the superatom-network (SAN) model.[43] The $Au_8^{4+}$ core of the three clusters should be viewed as two nonconjugate 4-center 2-electron (4c-2e) tetrahedral $Au_4$ superatoms.

Despite that there has been major progress in resolving the structure of ligand-protected gold clusters, there is still little known about the size evolution of superatoms in ligand-protected gold clusters in general because of the limited experimental data on structures of gold clusters in the small-to-medium size range. For 2e-superatomic Au-L nanoclusters, only two compounds[7,39] have been observed. It is significant for us to make predictions of 2e clusters and find the growth mechanism of them, which can lead to some preparations for 2e-superatomic Au-L clusters in future experiments. In this work, we report a systematic study of low-lying structures of 2e-superatomic ligand-protected Au nanoclusters: $Au_2\text{-}(AuL)_{1-12}$ (L = Cl, SH, $SCH_3$, $PH_2$, and $P(CH_3)_2$). Major attention is placed on the search for structures of the lowest-energy clusters of $Au_2\text{-}(AuL)_{1-12}$. The structures of $Au_2\text{-}(AuL)_{1-12}$ nanoclusters with five different ligands are given, and the size evolution of the 2e-superatom Au cores can be seen clearly. We think that the size evolution of the 2e-superatom is significant for small size ligand-protected Au clusters, which can be useful in predicting the structures of Au-L nanoclusters with a magic number of 2 and understanding the evolution of the superatom.

## 2. COMPUTATIONAL METHODS

The geometries of $Au_2\text{-}(AuCl)_{1-12}$ are located by using the method combining the genetic algorithm (GA) with DFT implemented in our group, which has been successfully applied in the structural prediction of a number of systems.[44−48] GAs belong to a larger class of evolutionary algorithms, which generate solutions to optimization problems using techniques inspired by natural evolution, such as inheritance, mutation, selection, and crossover.[49,50] All our DFT computations were accomplished by the GAUSSIAN09 package[51] using the TPSS functional.[52] The TPSS functional was proven to give reasonably accurate energetic properties of small Au clusters.[53−57] In global research of the potential energy surface, the sto-3g and LanL2MB basis sets are employed for ligands (L = Cl, SH, $SCH_3$, $PH_2$, $P(CH_3)_2$) and metals (Au), respectively. After global optimizations, the low-lying isomers are fully relaxed at the TPSS/6-31G*/LanL2DZ levels. The calculations of molecular orbital (MO) and the natural bond orbital (NBO)[58] analyses are also calculated at the same level. Molecular visualization is performed using MOLEKEL 5.4.[59]

## 3. RESULTS AND DISCUSSION

**A. Geometric Structures.** Using the combination of GA and DFT, we obtained a series of structures for $Au_2\text{-}(AuL)_{1-12}$ (L = Cl, SH, $SCH_3$, $PH_2$, and $P(CH_3)_2$) clusters at the TPSS/6-31G*/Lanl2DZ level. The lowest-lying equilibrium geometries and their symmetries of these clusters are shown. It is worth noting that there are too many isomers for each cluster, and showing isomers of each cluster is meaningless for discussing the size evolution of superatoms (other low-lying isomers are available in the Supporting Information, SI).

*$Au_2\text{-}(AuCl)_n$ (n = 1−12).* The most stable geometries of $Au_2\text{-}(AuCl)_n$ ($n$ = 1−12) clusters are shown in Figure 1. We

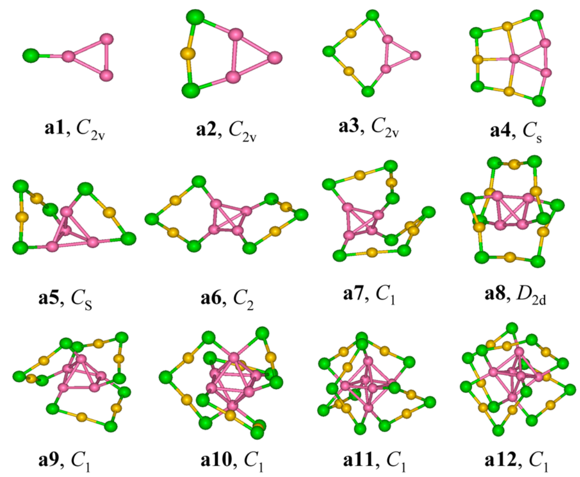


**Figure 1.** Putative global minima of $Au_2\text{-}(AuCl)_n$ ($n$ = 1−12) clusters, and the symmetries are labeled. Au, yellow; Cl, green. The superatomic Au cores are shown in pink.

emphasize the color of Au cores as pink of each structure in order to see it more clearly. When $n$ = 1−4, the Au cores of **a1** to **a4** ($Au_2\text{-}(AuCl)_{1-4}$) are triangle ($Au_3$) covered by one staple motif with different lengths, −Cl−, −Cl−Au−Cl− (monomer), −Cl−Au−Cl−Au−Cl− (dimer), and −Cl−Au−Cl−Au−Cl−Au−Cl− (trimer), respectively. Such a $Au_3$ 2e-superatom has not been viewed in the experimentally produced Au-L clusters. One atom of the Au core is isolated of **a1**, **a2**, and **a3**, so they disagree with the "divide-and-protect" model; however, **a4** follows the model because the isolated Au is protected by Au···Au contact. For **a5** to **a8** [$Au_2\text{-}(AuCl)_{5-8}$], each cluster contains a core of $Au_4$ tetrahedron protected by two staple motifs each connecting two next-nearest-neighbor vertices of the tetrahedron, which follows the "divide-and-protect" model. Note that the tetrahedral $Au_4$ core has been predicted by DFT calculations, such as in $Au_{10}(SR)_8$[41] and $Au_8(SR)_6$.[42] Interestingly, **a8** has a $Au_4$ core with two interlocking trimer motifs and in a high $D_{2d}$ symmetry. These interlocking staple motifs were previously viewed in some Au-L clusters, such as $Au_{22}(SR)_{18}$[60] and $Au_{24}(SR)_{20}$.[32] When $n$ = 9−12, the regularity of two motifs each connecting two next-nearest-neighbor vertices of the Au cores is broken, of which one vertex in the Au cores can be connected with two staple motifs, which does not follow the "divide-and-protect" model. **a9** has an irregular pentahedral ($Au_5$) core covered by three dimer motifs. Such a $Au_5$ 2e-superatom has not been viewed in the experimentally produced Au-L clusters. From **a10** to **a12**, each compound contains a $Au_6$ octahedron protected by four motifs. Such a $Au_6$ kernel is consistent with the structure of the $Au_{12}(SR)_9^+$ cluster.[31] From above, it is noted that those staple motifs ($-Au_n\text{-}Cl_{(n+1)}-$) have not been observed experimentally in ligand-protected Au nanoclusters.


DOI: 10.1021/acs.jpcc.5b10612
J. Phys. Chem. C 2016, 120, 2432−2438

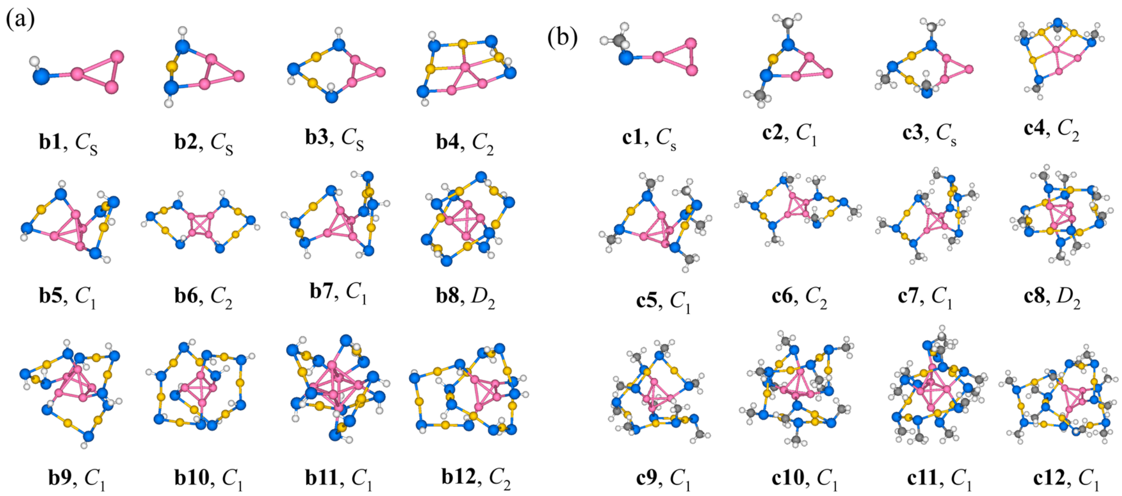


**Figure 2.** Putative global minima of (a) $Au_2$-$(AuSH)_n$ and (b) $Au_2$-$(AuSCH_3)_n$ ($n$ = 1−12) clusters, and the symmetries are labeled. Au, yellow; S, blue; C, black; H, white. The superatomic Au cores are shown in pink.

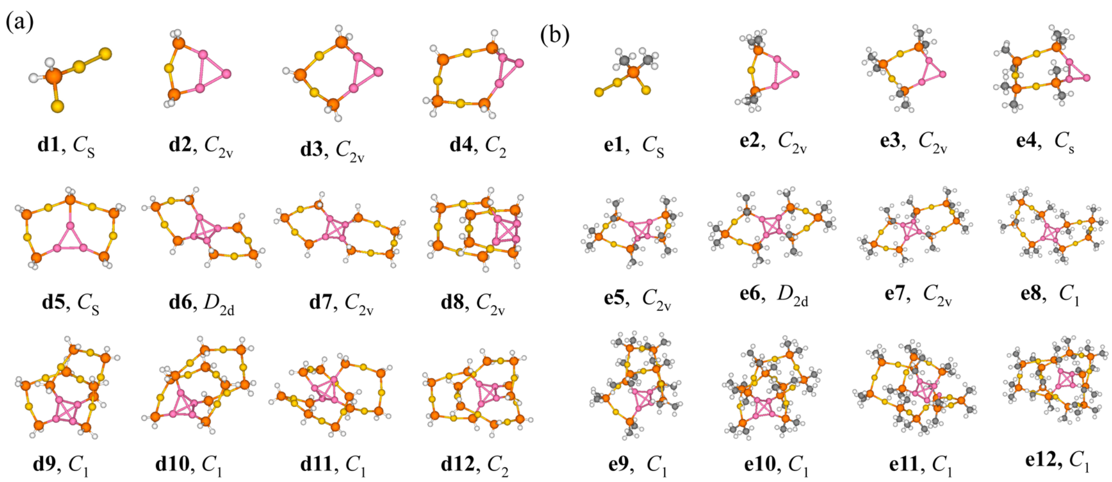


**Figure 3.** Putative global minima of (a) $Au_2$-$(AuPH_2)_n$ and (b) $Au_2$-$(AuP(CH_3)_2)_n$ ($n$ = 1−12) clusters, and the symmetries are labeled. Au, yellow; P, orange; C, black; H, white. The superatomic Au cores are shown in pink.

*$Au_2$-$(AuSH)_n$ ($n$ = 1−12).* The putative global minima (GM) of $Au_2$-$(AuSH)_n$ ($n$ = 1−12) clusters are shown in Figure 2a. When $n$ = 1−9, their structural frameworks are the same as those of **a1** to **a9** discussed above. The Au cores are triangle ($Au_3$) from **b1** to **b4** and tetrahedron ($Au_4$) from **b5** to **b9**. For $Au_8(AuSH)_6$ (**b6**), two trimer motifs wrap around two faces of the tetrahedron and connect two vertices, which agrees with the prediction in ref 42. **b8** has a $Au_4$ core with two interlocking trimer motifs and in a high $D_{2d}$ symmetry, which is in agreement with the structure predicted in ref 41. $Au_{12}(AuSH)_{10}$ (**b10**) is also the tetrahedral core ($Au_4$) surrounded by two $Au_4(SH)_5$ motifs. **b11** can be viewed as an octahedral ($Au_6$) core stapled by three dimer units and one monomer unit, where two vertices of the octahedron are overprotected. **b12** consists of a tetrahedral ($Au_4$) core protected by one $-Au_7(SH)_9-$ and one $-Au_3(SH)_5-$ motifs, where the pattern for the interlocking staple motifs is similar to that in the $Au_{24}(SR)_{20}$ cluster.[61]

*$Au_2$-$(AuSCH_3)_n$ ($n$ = 1−12).* The putative global minima are shown in Figure 2b. The structural frameworks are very similar to $Au_2$-$(AuSH)_n$ clusters, and the global minimum structures are different only at $n$ = 9 and 11. **c9** consists of a tetrahedral ($Au_4$) core surrounded by one $-SCH_3-(AuSCH_3)_5-$ and one dimer staple, which is in agreement with the structure predicted in ref 39. The core in **c11** is a trigonal bipyramid ($Au_5$) which is protected by two trimer and one dimer motifs.

*$Au_2$-$(AuPH_2)_n$ ($n$ = 1−12).* The most stable geometries of $Au_2$-$(AuPH_2)_n$ ($n$ = 1−12) clusters are shown in Figure 3a. Different from L = Cl and SH, the $Au_3$ triangular core is broken at $n$ = 1 (**d1**). The GM structures are quasiplanar up to $n$ = 5 (one $Au_3$ triangular core protected by one staple motif), where there is a long staple motif $(-PH_2$-$(AuPH_2)_4-)$ in **d5**. When $n$ = 6−12, each structure follows the "divide-and-protect" model which contains a tetrahedral $Au_4$ core and an outside protective layer of two staple motifs. **d6** is a tetrahedron core ($Au_4$) protected by two dimer units in $C_{2v}$ symmetry. **d7** is covered by one dimer and one trimer motif. **d8** is a tetrahedron core protected by two interlocking trimer units in $C_{2v}$ symmetry. **d9** is a $Au_4$ core stapled by one $Au_3(PH_2)_4$ and one $Au_4(PH_2)_5$ oligomer. **d10** is protected by two $-PH_2$-$(AuPH_2)_4-$ staple motifs. **d11** is a $Au_4$ core covered by one trimer and one long $-PH_2$-$(AuPH_2)_6-$ unit. **d12** is a tetrahedral core stapled by one trimer and one long $-PH_2$-$(AuPH_2)_7-$ motif. We find that the experimentally produced $Au_{24}(SR)_{20}$ cluster[61] can be viewed as two $Au_4$ cores protected by four interlocking motifs, and **d12**


DOI: 10.1021/acs.jpcc.5b10612
J. Phys. Chem. C 2016, 120, 2432−2438

has the same structure feature with one-half of the $Au_{24}(SR)_{20}$ cluster.

*$Au_2$-$(AuP(CH_3)_2)_n$ ($n$ = 1−12).* The putative global minima are shown in Figure 3b. As the ligand changed from $PH_2$ to $P(CH_3)_2$, the skeleton of the structures does not change at $n$ = 1−4. The Au core in **e5** is a tetrahedron ($Au_4$), but that in **d5** is a triangle ($Au_3$) core. At $n$ = 6−12, the GM structures are very similar to L = $PH_2$ (one tetrahedron core protected by two staple motifs), and only the length of some staple motifs is changed. The two staples in **e8** are not interlocking due to steric effect. **e11** is a $Au_4$ core covered by one dimer motif and one long $-PH_2$-$(AuPH_2)_7-$ staple. Similar to L = Cl, those staple motifs ($-Au_n$-$[PH_2]_{(n+1)}-$, $-Au_m$-$[P(CH_3)_2]_{(m+1)}-$) also have not been observed experimentally in Au-L nanoclusters.

From the above analysis, we can see that each of these Au-L clusters has one Au core ($Au_3$, $Au_4$, $Au_5$, or $Au_6$) covered by one to four staple motifs except $Au_2$-$(AuPH_2)$ and $Au_2$-$(AuP(CH_3)_2)$ clusters. When cluster size is small, the structures are (quasi-)planar, and they just follow the superatom model but disagree with the "divide-and-protect" model. The GM structures change from (quasi-)planar to three-dimensional with cluster size increasing. Ligand effects are also very important for Au-L clusters. The structural frameworks of $Au_2$-$(AuSCH_3)_n$ clusters are very similar to $Au_2$-$(AuSH)_n$ clusters, so we can use SH to replace SR in DFT prediction for lower computational costs. Similarly, we can use $PH_2$ to replace $PR_2$ in structural predictions. For L = Cl, the Au cores of $Au_2$-$(AuCl)_n$ clusters tend to be large with cluster size increasing, and the length of the staple motifs of the clusters is preferred to be short (the longest staple is trimer). The "divide-and-protect" model is not maintained strictly in the Au−Cl structures due to the high polarity of Au−Cl bonds and the strong attraction of Au···Au contacts. However, for L = $PH_2$ and $P(CH_3)_2$, the Au cores in the clusters tend to be $Au_4$ following strictly the "divide-and-protect" model at large cluster sizes, and the length of staple motifs can be very long twining around the Au core. The reason may be that the Au−P bonds are of less polarity but the Au···Au contact is weaker compared to those in the Au−Cl system. For L = SH and $SCH_3$, structure features of the clusters fall in between those of L = Cl and L = $PH_2$, $P(CH_3)_2$, and the polarity of Au−S bonds and strength of Au···Au contacts in the Au−S system are in between.

**B. Stability.** In this part, the atomization energies (average interaction energy per Au-L formula unit in the cluster, $E_{at} = [E_{Au2\text{-}(AuL)n} - (n + 2)*E_{Au} - n*E_L]$), and the average energies (a four-parameter fitting of the GMs: $E_{ave} = a + bn^{1/3} + cn^{2/3} + dn$) of the clusters are calculated. The R groups do not affect much of the structure feature of the compounds, thus we just calculated the energies of $Au_2$-$(AuCl)_n$, $Au_2$-$(AuSH)_n$, and $Au_2$-$(AuPH_2)_n$ clusters. To show the relative stability of the global minimum structures at different cluster sizes, the energies ($E_{at} - E_{ave}$) of the GMs are depicted in Figure 4 in a manner that emphasizes particular stable minima or "magic numbers". In such a curve, upward peaks represent that the atomization energy is higher than the average, and the structure is more stable.

For L = Cl, Figure 4a shows upward peaks at $n$ = 2, 5, 8, and 11, indicating higher stability of $Au_2$-$(AuCl)_2$, $Au_2$-$(AuCl)_5$, $Au_2$-$(AuCl)_8$, and $Au_2$-$(AuCl)_{11}$ compared to other sizes. For L = SH, as shown in Figure 4b, there are obvious upward peaks at $n$ = 2 and 6, indicating relatively more stability of $Au_2$-$(AuSH)_2$ and $Au_2$-$(AuSH)_6$ clusters. For L = $PH_2$, the red curve shows that $Au_2$-$(AuPH_2)_3$, $Au_2$-$(AuPH_2)_6$, $Au_2$-$(AuPH_2)_7$, and $Au_2$-$(AuPH_2)_{12}$ clusters are stable "magic numbers". It is worth mentioning that $Au_2$-$(AuPH_2)_{12}$ is the most stable one in the $Au_2$-$(AuPH_2)_n$ system. Linking that **d12** has the same structural feature with experimentally produced $Au_{24}(SR)_{20}$ cluster, we infer that the $Au_2$-$(AuPH_2)_{12}$ cluster may be synthesized in the future.

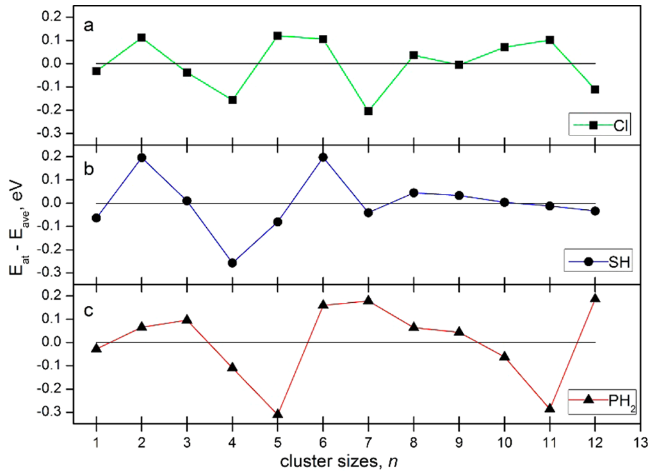


**Figure 4.** Plots of the energetic gaps ($E_{at} - E_{ave}$) of (a) $Au_2$-$(AuCl)_n$, (b) $Au_2$-$(AuSH)_n$, and (c) $Au_2$-$(AuPH_2)_n$ clusters as a function of cluster sizes $n$, where $E_{at}$ is the atomization energy ($E_{at} = [E_{Au2\text{-}(AuL)n} - (n + 2)*E_{Au} - n*E_L]$, L = Cl, SH, $PH_2$) and $E_{ave}$ is a four-parameter fitting of the GMs ($E_{ave} = a + bn^{1/3} + cn^{2/3} + dn$). Upward peaks represent that the atomization energy is higher than the average, and the structure is more stable.

**C. Aromaticity.** Aromaticity is a concept invented to account for the unusual stability of an important class of organic molecules. The nucleus-independent chemical shift (NICS) value is the most widely used as a quantitative measure for aromaticity (negative NICS values mean aromaticity, and positive NICS values mean antiaromaticity).[62] In 2001, Boldyrev and Wang et al. reported experimental and theoretical evidence of aromaticity in all-metal systems ($Al_4^{2-}$).[63] NICS values at the geometric centers of the rings [NICS(0)] were calculated, which are better suited for evaluation of the aromaticity for all-metal species.

Delocalization is always associated with aromaticity, and the delocalized $nc$-2e bonds should also be aromatic, so we calculated the NICS(0) values of superatoms of $Au_2$-$(AuCl)_n$, $Au_2$-$(AuSH)_n$, and $Au_2$-$(AuPH_2)_n$ clusters at the TPSS/6-31G*/Lanl2DZ level. Figure 5 plots the NICS(0) values as a function of the cluster sizes. For each cluster, the calculated NICS(0) values are largely negative (−40.3 to −22.1 ppm), suggesting very high aromaticity of the superatoms. Besides, the aromaticity of $Au_4$ superatoms is stronger than those of $Au_6$ superatoms. Interestingly, it is found that higher Au···Au aurophilic interaction may result in lower aromaticity. For example, $Au_2$-$(AuL)_8$ is a $Au_4$ core surrounded by two interlocking staple motifs with high Au···Au aurophilic interaction, and the aromaticity at $n$ = 8 is much lower than that at $n$ = 7 and 6. For quasiplanar structures, the Au···Au aurophilic interaction of **a3**, **b3**, and **d4** is high, and the aromaticity is lower than that of **a4**, **b4**, and **d5**, respectively. This indicates that Au···Au aurophilic interaction is a kind of non-Lewis interaction, which can affect the feature of the 2e-superatom.

**D. Electronic Structures.** Those compounds both have two free valence electrons in the gold core, which agree with


DOI: 10.1021/acs.jpcc.5b10612
J. Phys. Chem. C 2016, 120, 2432−2438

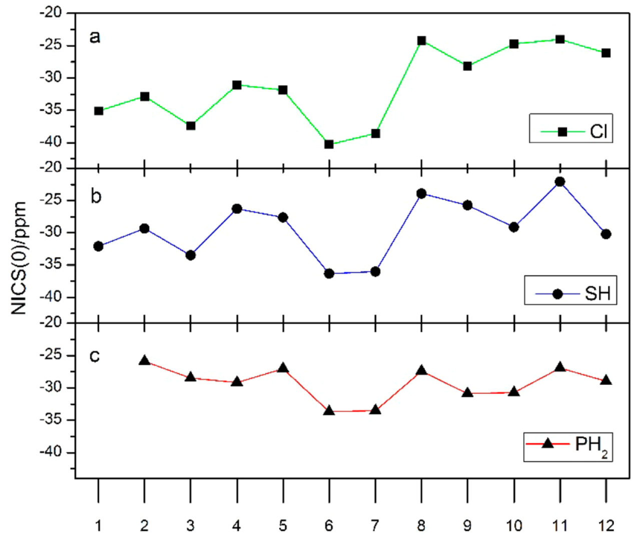


**Figure 5.** NICS(0) values of superatoms of (a) $Au_2$-$(AuCl)_n$ (green curve), (b) $Au_2$-$(AuSH)_n$ (blue curve), and (c) $Au_2$-$(AuPH_2)_n$ (red curve) clusters and as a function of cluster sizes $n$.

the counts of magic number 2 in the superatom model. To give a direct evidence of the existence of these superatoms, the adaptive natural density partitioning (AdNDP) is used to analyze the chemical bonding. This method was developed by Zubarev and Boldyrev[64] and used to analyze chemical bonding in organic molecules, boron clusters, and Au clusters.[54,55,65−67] The AdNDP method is based on the concept of the electron pair as the main element of chemical bonding models, which recovers both Lewis bonding elements (1c-2e and 2c-2e objects) and delocalized bonding elements ($n$c-2e).

The results of $n$c-2e delocalized superatomic orbitals in (a) $Au_2$-$(AuCl)_{1-12}$, (b) $Au_2$-$(AuSH)_{1-12}$, and (c) $Au_2$-$(AuPH_2)_{1-12}$ clusters are displayed in Figure 6. AdNDP analysis reveals one 2c−2e (two centers and two electrons) bond in **d1**; one 3c−2e (three centers and two electrons) bond in **a1** to a4, **b1** to **b4**, and **d2** to **d5**; one 4c−2e bond in **a5** to **a8**, **b5** to **b8**, **b10** and **b12**, and **d6** to **d12**; one 5c−2e bond in **a9** and **b9**; and one 6c−2e bond in **a10** to **a12** and **b11**. The results of AdNDP chemical bonding confirm the existences of superatoms in our Au-L nanocluster systems. Moreover, we note the occupancy numbers (ONs) are of a wide difference of these compounds. Similar to aromaticity, the ONs of the delocalized superatomic 2e-bonding can also be affected by aurophilic interactions, in which higher Au···Au aurophilic interactions may result in lower ONs. For example, the ON at $n$ = 8 is obviously lower than that at $n$ = 6 and 7. Besides, the ON of **a3**, **b3**, and **d4** is obviously higher than **a4**, **b4**, and **d5**, respectively. This indicates that although Au···Au aurophilic interaction is a kind of non-Lewis interaction it is rather strong and can clearly affect the superatomic 2e-bonding.

## 4. CONCLUSIONS

In this work, the superatomic structures of $Au_2$-$(AuL)_{1-12}$ (L = Cl, SH, $SCH_3$, $PH_2$, $P(CH_3)_2$) clusters have been studied. These compounds have two free valence electrons in the gold core, which agree with the counts of magic number 2 in the superatom model. The putative GM structures of these clusters are investigated using the combination of genetic algorithm (GA) and DFT method, relying on TPSS functional. Each of these Au-L clusters has one Au core ($Au_3$, $Au_4$, $Au_5$, or $Au_6$) covered by one to four staple motifs except $Au_2$-$AuPH_2$ and $Au_2$-$AuP(CH_3)_2$. The GM structures change from (quasi)-planar to three-dimensional with cluster size increasing, and these compounds basically follow the "divide-and-protect" model. Ligand effects of the structures are also analysised. For L = Cl, because the polarity of the Au−Cl bond is high and aurophilic interaction is strong, the Au cores tend to be large with increasing cluster size, and the length of the staple motifs is preferred to be short. For L = $PR_2$, the picture is reversed because of the low polarity of the Au−P bond and weak aurophilic interaction. Direct evidence for the existence of 2e-superatoms is given by chemical bonding analysis using the AdNDP method. The aromatic properties of the superatoms have been explored by the NICS method, which indicates that the 2e-superatoms are highly aromatic. The Au···Au aurophilic

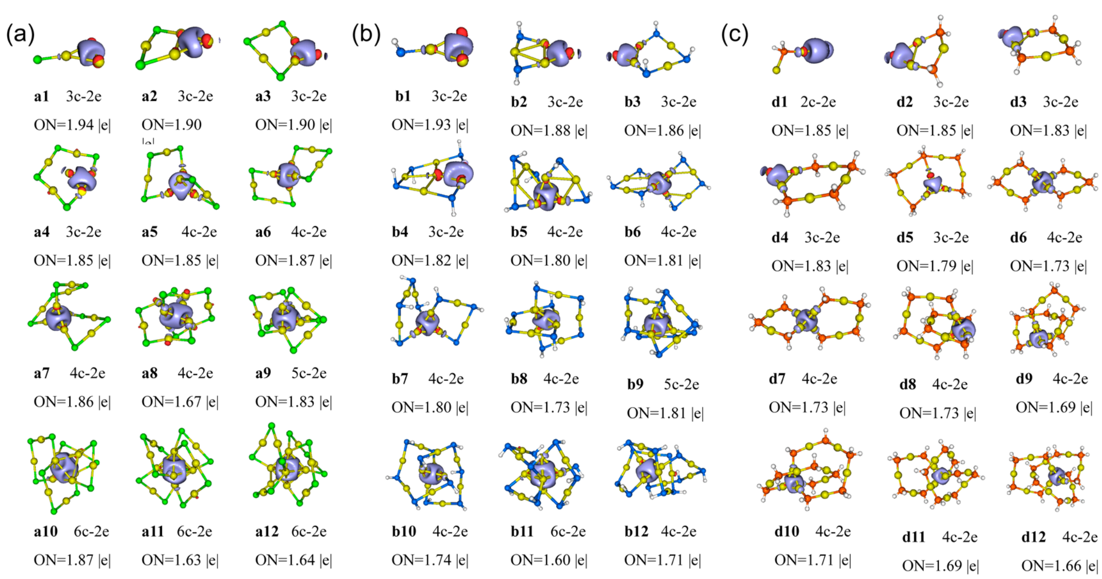


**Figure 6.** AdNDP localized natural bonding of the $n$c-2e delocalized superatomic orbitals in (a) $Au_2$-$(AuCl)_n$ (**a1**−**a12**), (b) $Au_2$-$(AuSH)_n$ (**b1**−**b12**), and (c) $Au_2$-$(AuPH_2)_n$ (**d1**−**d12**) clusters. Au, yellow; Cl, green; S, blue; P, orange; H, white.


DOI: 10.1021/acs.jpcc.5b10612
J. Phys. Chem. C 2016, 120, 2432−2438

interaction is a kind of non-Lewis interaction; however, it can clearly weaken the aromaticity and ONs of the superatomic 2e-bonding. This work gives a direct and overall view of size evolution of 2e-superatoms in Au-L clusters, which gives some new perspectives in terms of how Au-L nanoclusters change with increasing cluster size.

## ■ ASSOCIATED CONTENT

### Supporting Information

The Supporting Information is available free of charge on the ACS Publications website at DOI: 10.1021/acs.jpcc.5b10612.

Structures and energies of the located global minimum and low-energy isomers of $Au_2$-$(AuL)_{1-12}$ clusters, with L = Cl, SH, $SCH_3$, $PH_2$, and $P(CH_3)_2$, respectively (PDF)

## ■ AUTHOR INFORMATION

### Corresponding Author

*E-mail: clj@ustc.edu.

### Author Contributions

The manuscript was written through contributions of all authors. All authors have given approval to the final version of the manuscript.

### Notes

The authors declare no competing financial interest.

## ■ ACKNOWLEDGMENTS

This work is financed by the National Natural Science Foundation of China (21273008, 21573001) and by the CSC. The calculations were carried out at the High-Performance Computing Center of Anhui University.

## ■ REFERENCES

(1) Ingram, R. S.; Hostetler, M. J.; Murray, R. W.; Schaaff, T. G.; Khoury, J. T.; Whetten, R. L.; Bigioni, T. P.; Guthrie, D. K.; First, P. N. 28 Kda Alkanethiolate-Protected Au Clusters Give Analogous Solution Electrochemistry and Stm Coulomb Staircases. *J. Am. Chem. Soc.* **1997**, *119*, 9279−9280.

(2) Chen, S.; Ingram, R. S.; Hostetler, M. J.; Pietron, J. J.; Murray, R. W.; Schaaff, T. G.; Khoury, J. T.; Alvarez, M. M.; Whetten, R. L. Gold Nanoelectrodes of Varied Size: Transition to Molecule-Like Charging. *Science* **1998**, *280*, 2098−2101.

(3) Wuelfing, W. P.; Gross, S. M.; Miles, D. T.; Murray, R. W. Nanometer Gold Clusters Protected by Surface-Bound Monolayers of Thiolated Poly (Ethylene Glycol) Polymer Electrolyte. *J. Am. Chem. Soc.* **1998**, *120*, 12696−12697.

(4) Hostetler, M. J.; Templeton, A. C.; Murray, R. W. Dynamics of Place-Exchange Reactions on Monolayer-Protected Gold Cluster Molecules. *Langmuir* **1999**, *15*, 3782−3789.

(5) Templeton, A. C.; Wuelfing, W. P.; Murray, R. W. Monolayer-Protected Cluster Molecules. *Acc. Chem. Res.* **2000**, *33*, 27−36.

(6) Jana, N. R.; Gearheart, L.; Murphy, C. J. Seeding Growth for Size Control of 5−40 nm Diameter Gold Nanoparticles. *Langmuir* **2001**, *17*, 6782−6786.

(7) Negishi, Y.; Nobusada, K.; Tsukuda, T. Glutathione-Protected Gold Clusters Revisited: Bridging the Gap between Gold(I)-Thiolate Complexes and Thiolate-Protected Gold Nanocrystals. *J. Am. Chem. Soc.* **2005**, *127*, 5261−5270.

(8) Chaki, N. K.; Tsunoyama, H.; Negishi, Y.; Sakurai, H.; Tsukuda, T. Effect of Ag-Doping on the Catalytic Activity of Polymer-Stabilized Au Clusters in Aerobic Oxidation of Alcohol. *J. Phys. Chem. C* **2007**, *111*, 4885−4888.

(9) Lopez-Acevedo, O.; Kacprzak, K. A.; Akola, J.; Häkkinen, H. Quantum Size Effects in Ambient Co Oxidation Catalysed by Ligand-Protected Gold Clusters. *Nat. Chem.* **2010**, *2*, 329−334.

(10) Jiang, D. E.; Walter, M. The Halogen Analogs of Thiolated Gold Nanoclusters. *Nanoscale* **2012**, *4*, 4234−4239.

(11) Jin, R. Quantum Sized, Thiolate-Protected Gold Nanoclusters. *Nanoscale* **2010**, *2*, 343−362.

(12) Jin, R. Atomically Precise Metal Nanoclusters: Stable Sizes and Optical Properties. *Nanoscale* **2015**, *7*, 1549−1565.

(13) Jadzinsky, P. D.; Calero, G.; Ackerson, C. J.; Bushnell, D. A.; Kornberg, R. D. Structure of a Thiol Monolayer-Protected Gold Nanoparticle at 1.1 a Resolution. *Science* **2007**, *318*, 430−433.

(14) Zhu, M.; Aikens, C. M.; Hollander, F. J.; Schatz, G. C.; Jin, R. Correlating the Crystal Structure of a Thiol-Protected $Au_{25}$ Cluster and Optical Properties. *J. Am. Chem. Soc.* **2008**, *130*, 5883−5885.

(15) Heaven, M. W.; Dass, A.; White, P. S.; Holt, K. M.; Murray, R. W. Crystal Structure of the Gold Nanoparticle $[N(C_8H_{17})_4]$-$[Au_{25}(SCH_2CH_2Ph)_{18}]$. *J. Am. Chem. Soc.* **2008**, *130*, 3754−3755.

(16) Hakkinen, H.; Walter, M.; Gronbeck, H. Divide and Protect: Capping Gold Nanoclusters with Molecular Gold-Thiolate Rings. *J. Phys. Chem. B* **2006**, *110*, 9927−9931.

(17) Qian, H.; Eckenhoff, W. T.; Zhu, Y.; Pintauer, T.; Jin, R. Total Structure Determination of Thiolate-Protected $Au_{38}$ Nanoparticles. *J. Am. Chem. Soc.* **2010**, *132*, 8280−8281.

(18) Price, R. C.; Whetten, R. L. All-Aromatic, Nanometer-Scale, Gold-Cluster Thiolate Complexes. *J. Am. Chem. Soc.* **2005**, *127*, 13750−13751.

(19) Nimmala, P. R.; Dass, A. $Au_{36}(SPh)_{23}$ Nanomolecules. *J. Am. Chem. Soc.* **2011**, *133*, 9175−9177.

(20) Chevrier, D. M.; MacDonald, M. A.; Chatt, A.; Zhang, P.; Wu, Z.; Jin, R. Sensitivity of Structural and Electronic Properties of Gold−Thiolate Nanoclusters to the Atomic Composition: A Comparative X-Ray Study of $Au_{19}(SR)_{13}$ and $Au_{25}(SR)_{18}$. *J. Phys. Chem. C* **2012**, *116*, 25137−25142.

(21) Chen, S.; Wang, S.; Zhong, J.; Song, Y.; Zhang, J.; Sheng, H.; Pei, Y.; Zhu, M. The Structure and Optical Properties of the $[Au_{18}(SR)_{14}]$ Nanocluster. *Angew. Chem., Int. Ed.* **2015**, *54*, 3145−3149.

(22) Azubel, M.; Koivisto, J.; Malola, S.; et al. Electron Microscopy of Gold Nanoparticles at Atomic Resolution. *Science* **2014**, *345*, 909−912.

(23) Crasto, D.; Malola, S.; Brosofsky, G.; Dass, A.; Hakkinen, H. Single Crystal XRD Structure and Theoretical Analysis of the Chiral $Au_{30}S(S\text{-}t\text{-}Bu)_{18}$ Cluster. *J. Am. Chem. Soc.* **2014**, *136*, 5000−5005.

(24) Zeng, C.; Li, T.; Das, A.; Rosi, N. L.; Jin, R. Chiral Structure of Thiolate-Protected 28-Gold-Atom Nanocluster Determined by X-ray Crystallography. *J. Am. Chem. Soc.* **2013**, *135*, 10011−10013.

(25) Zeng, C.; Chen, Y.; Kirschbaum, K.; Appavoo, K.; Sfeir, M. Y.; Jin, R. Structural Patterns at All Scales in a Nonmetallic Chiral $Au_{133}(SR)_{52}$ Nanoparticle. *Sci. Adv.* **2015**, *1*, e1500045.

(26) Dass, A.; Theivendran, S.; Nimmala, P. R.; Kumara, C.; Jupally, V. R.; Fortunelli, A.; Sementa, L.; Barcaro, G.; Zuo, X.; Noll, B. C. Au133(SPh-tBu)52 Nanomolecules: X-ray Crystallography, Optical, Electrochemical, and Theoretical Analysis. *J. Am. Chem. Soc.* **2015**, *137*, 4610−4613.

(27) Zeng, C.; Chen, Y.; Li, G.; Jin, R. Synthesis of a $Au_{44}(SR)_{28}$ Nanocluster: Structure Prediction and Evolution from $Au_{28}(SR)_{20}$, $Au_{36}(SR)_{24}$ to $Au_{44}(SR)_{28}$. *Chem. Commun.* **2014**, *50*, 55−57.

(28) Akola, J.; Walter, M.; Whetten, R. L.; Hakkinen, H.; Gronbeck, H. On the Structure of Thiolate-Protected $Au_{25}$. *J. Am. Chem. Soc.* **2008**, *130*, 3756−3757.

(29) Guerra, C. F.; Snijders, J.; Te Velde, G.; Baerends, E. Towards an Order-N DFT Method. *Theor. Chem. Acc.* **1998**, *99*, 391−403.

(30) Lopez-Acevedo, O.; Akola, J.; Whetten, R. L.; Gronbeck, H.; Häkkinen, H. Structure and Bonding in the Ubiquitous Icosahedral Metallic Gold Cluster $Au_{144}(SR)_{60}$. *J. Phys. Chem. C* **2009**, *113*, 5035−5038.

(31) Jiang, D.-e.; Whetten, R. L.; Luo, W.; Dai, S. The Smallest Thiolated Gold Superatom Complexes. *J. Phys. Chem. C* **2009**, *113*, 17291−17295.

(32) Pei, Y.; Pal, R.; Liu, C. Y.; Gao, Y.; Zhang, Z. H.; Zeng, X. C. Interlocked Catenane-Like Structure Predicted in $Au_{24}(SR)_{20}$:

Implication to Structural Evolution of Thiolated Gold Clusters from Homoleptic Gold(I) Thiolates to Core-Stacked Nanoparticles. *J. Am. Chem. Soc.* **2012**, *134*, 3015−3024.
(33) Tlahuice, A.; Garzón, I. L. On the Structure of the $Au_{18}(SR)_{14}$ Cluster. *Phys. Chem. Chem. Phys.* **2012**, *14*, 3737−3740.
(34) Xu, W. W.; Gao, Y.; Zeng, X. C. Unraveling Structures of Protection Ligands on Gold Nanoparticle $Au_{68}(SH)_{32}$. *Sci. Adv.* **2015**, *1*, e1400211.
(35) Xu, W. W.; Gao, Y. Unraveling the Atomic Structures of the $Au_{68}(SR)_{34}$ Nanoparticles. *J. Phys. Chem. C* **2015**, *119*, 14224−14229.
(36) Pei, Y.; Lin, S.; Su, J.; Liu, C. Structure Prediction of $Au_{44}(SR)_{28}$: A Chiral Superatom Cluster. *J. Am. Chem. Soc.* **2013**, *135*, 19060−19063.
(37) Walter, M.; Akola, J.; Lopez-Acevedo, O.; Jadzinsky, P. D.; Calero, G.; Ackerson, C. J.; Whetten, R. L.; Gronbeck, H.; Häkkinen, H. A Unified View of Ligand-Protected Gold Clusters as Superatom Complexes. *Proc. Natl. Acad. Sci. U. S. A.* **2008**, *105*, 9157−9162.
(38) Dass, A. Mass Spectrometric Identification of $Au_{68}(SR)_{34}$ Molecular Gold Nanoclusters with 34-Electron Shell Closing. *J. Am. Chem. Soc.* **2009**, *131*, 11666−11667.
(39) Luo, Z.; Nachammai, V.; Zhang, B.; Yan, N.; Leong, D. T.; Jiang, D. E.; Xie, J. Toward Understanding the Growth Mechanism: Tracing All Stable Intermediate Species from Reduction of Au (I)−thiolate Complexes to Evolution of Au25 Nanoclusters. *J. Am. Chem. Soc.* **2014**, *136*, 10577−10580.
(40) Jiang, D. E.; Overbury, S. H.; Dai, S. Structure of $Au_{15}(SR)_{13}$ and Its Implication for the Origin of the Nucleus in Thiolated Gold Nanoclusters. *J. Am. Chem. Soc.* **2013**, *135*, 8786−8789.
(41) Jiang, D.-e.; Chen, W.; Whetten, R. L.; Chen, Z. What Protects the Core When the Thiolated Au Cluster Is Extremely Small? *J. Phys. Chem. C* **2009**, *113*, 16983−16987.
(42) Jiang, D. E.; Whetten, R. L.; Luo, W.; Dai, S. The Smallest Thiolated Gold Superatom Complexes. *J. Phys. Chem. C* **2009**, *113*, 17291−17295.
(43) Cheng, L.; Yuan, Y.; Zhang, X.; Yang, J. Superatom Networks in Thiolate-Protected Gold Nanoparticles. *Angew. Chem., Int. Ed.* **2013**, *52*, 9035−9039.
(44) Li, L.; Xu, C.; Jin, B.; Cheng, L. Benzene Analogues of (Quasi-) Planar $M@B_nH_n$ Compounds ($M = V^-$, Cr, $Mn^+$): A Theoretical Investigation. *J. Chem. Phys.* **2013**, *139*, 174310.
(45) Li, L.; Xu, C.; Jin, B.; Cheng, L. Ferrocene Analogues of Sandwich M $(CrB_6H_6)_2$: A Theoretical Investigation. *Dalton Trans.* **2014**, *43*, 11739−11744.
(46) Li, R.; Cheng, L. Structural Determination of $(Al_2O_3)_N$ (N = 1−7) Clusters Based on Density Functional Calculation. *Comput. Theor. Chem.* **2012**, *996*, 125−131.
(47) Ren, L.; Cheng, L.; Feng, Y.; Wang, X. Geometric and Electronic Structures of $(BeO)_N$ (N = 2−12, 16, 20, and 24): Rings, Double Rings, and Cages. *J. Chem. Phys.* **2012**, *137*, 014309.
(48) Yuan, Y.; Cheng, L. Theoretical Prediction for the Structures of Gas Phase Lithium Oxide Clusters:$(Li_2O)_N$ (N = 1−8). *Int. J. Quantum Chem.* **2013**, *113*, 1264−1271.
(49) Johnston, R. L. Evolving Better Nanoparticles: Genetic Algorithms for Optimising Cluster Geometries. *Dalton Trans.* **2003**, 4193−4207.
(50) Shayeghi, A.; Götz, D.; Davis, J.; Schaefer, R.; Johnston, R. L. Pool-Bcga: A Parallelised Generation-Free Genetic Algorithm for the Ab Initio Global Optimisation of Nanoalloy Clusters. *Phys. Chem. Chem. Phys.* **2015**, *17*, 2104−2112.
(51) Frisch, M.; Trucks, G.; Schlegel, H. B.; Scuseria, G.; Robb, M.; Cheeseman, J.; Scalmani, G.; Barone, V.; Mennucci, B.; Petersson, G., et al. *Gaussian 09*, Revision A. 02; Gaussian. Inc.: Wallingford, CT, 2009.
(52) Tao, J.; Perdew, J. P.; Staroverov, V. N.; Scuseria, G. E. Climbing the Density Functional Ladder: Nonempirical Meta−Generalized Gradient Approximation Designed for Molecules and Solids. *Phys. Rev. Lett.* **2003**, *91*, 146401.
(53) Cheng, L.; Ren, C.; Zhang, X.; Yang, J. New Insight into the Electronic Shell of $Au_{38}(SR)_{24}$: A Superatomic Molecule. *Nanoscale* **2013**, *5*, 1475−1478.
(54) Cheng, L.; Zhang, X.; Jin, B.; Yang, J. Superatom−Atom Super-Bonding in Metallic Clusters: A New Look to the Mystery of an $Au_{20}$ Pyramid. *Nanoscale* **2014**, *6*, 12440−12444.
(55) Feng, Y.; Cheng, L. Structural Evolution of $(Au_2S)_N$ (N = 1−8) Clusters from First Principles Global Optimization. *RSC Adv.* **2015**, *5*, 62543−62550.
(56) Tian, Z.; Cheng, L. Perspectives on the Energy Landscape of Au−Cl Binary Systems from the Structural Phase Diagram of $Au_XCl_Y$ (X+Y = 20). *Phys. Chem. Chem. Phys.* **2015**, *17*, 13421−13428.
(57) Yuan, Y.; Cheng, L.; Yang, J. Electronic Stability of Phosphine-Protected $Au_{20}$ Nanocluster: Superatomic Bonding. *J. Phys. Chem. C* **2013**, *117*, 13276−13282.
(58) Glendening, E.; Badenhoop, J.; Reed, A.; Carpenter, J.; Bohmann, J.; Morales, C.; Weinhold, F. *NBO 5.0*; Theoretical Chemistry Institute, University of Wisconsin: Madison, 2001.
(59) Varetto, U. *Molekel 5.4.0.8*; Swiss National Supercomputing Centre: Manno, Switzerland, 2009.
(60) Yu, Y.; Luo, Z.; Chevrier, D. M.; Leong, D. T.; Zhang, P.; Jiang, D. E.; Xie, J. Identification of a Highly Luminescent $Au_{22}(SG)_{18}$ Nanocluster. *J. Am. Chem. Soc.* **2014**, *136*, 1246−1249.
(61) Das, A.; Li, T.; Li, G.; Nobusada, K.; Zeng, C.; Rosi, N. L.; Jin, R. Crystal Structure and Electronic Properties of a Thiolate-Protected $Au_{24}$ Nanocluster. *Nanoscale* **2014**, *6*, 6458−6462.
(62) Schleyer, P.; Maerker, C.; Dransfeld, A.; Jiao, H.; Hommes, N. Nucleus-Independent Chemical Shifts: A Simple and Efficient Aromaticity Probe. *J. Am. Chem. Soc.* **1996**, *118*, 6317−6318.
(63) Li, X.; Kuznetsov, A. E.; Zhang, H.-F.; Boldyrev, A. I.; Wang, L. S. Observation of All-Metal Aromatic Molecules. *Science* **2001**, *291*, 859−861.
(64) Zubarev, D. Y.; Boldyrev, A. I. Developing Paradigms of Chemical Bonding: Adaptive Natural Density Partitioning. *Phys. Chem. Chem. Phys.* **2008**, *10*, 5207−5217.
(65) Galeev, T. R.; Chen, Q.; Guo, J.-C.; Bai, H.; Miao, C. Q.; Lu, H. G.; Sergeeva, A. P.; Li, S.-D.; Boldyrev, A. I. Deciphering the Mystery of Hexagon Holes in an All-Boron Graphene A-Sheet. *Phys. Chem. Chem. Phys.* **2011**, *13*, 11575−11578.
(66) Li, D. Z.; Chen, Q.; Wu, Y. B.; Lu, H. G.; Li, S. D. Double-Chain Planar $D_{2h}B_4H_2$, $C_{2h}B_8H_2$, and $C_{2h}B_{12}H_2$: Conjugated Aromatic Borenes. *Phys. Chem. Chem. Phys.* **2012**, *14*, 14769−14774.
(67) Sergeeva, A. P.; Boldyrev, A. I. The Chemical Bonding of $Re_3Cl_9$ and Revealed by the Adaptive Natural Density Partitioning Aanlyses. *Comments Inorg. Chem.* **2010**, *31*, 2−12.


DOI: 10.1021/acs.jpcc.5b10612
*J. Phys. Chem. C* 2016, 120, 2432−2438